

Thermal stability of α -Ga₂O₃ films grown on c-plane sapphire substrates via mist-CVD

Cite as: AIP Advances **10**, 115013 (2020); <https://doi.org/10.1063/5.0020464>

Submitted: 10 October 2020 . Accepted: 15 October 2020 . Published Online: 10 November 2020

 Riena Jinno,  Kentaro Kaneko, and  Shizuo Fujita

COLLECTIONS

Paper published as part of the special topic on [Chemical Physics](#), [Energy, Fluids and Plasmas](#), [Materials Science](#) and [Mathematical Physics](#)



View Online



Export Citation



CrossMark

ARTICLES YOU MAY BE INTERESTED IN

[Growth mechanism of \$\alpha\$ -Ga₂O₃ on a sapphire substrate by mist chemical vapor deposition using acetylacetonated gallium source solutions](#)

Applied Physics Letters **117**, 052106 (2020); <https://doi.org/10.1063/5.0014056>

[Recent progress on the electronic structure, defect, and doping properties of Ga₂O₃](#)

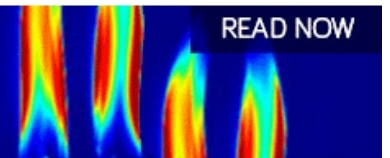
APL Materials **8**, 020906 (2020); <https://doi.org/10.1063/1.5142999>

[Halide vapor phase epitaxial growth of \$\beta\$ -Ga₂O₃ and \$\alpha\$ -Ga₂O₃ films](#)

APL Materials **7**, 022504 (2019); <https://doi.org/10.1063/1.5055680>

AIP Advances
Fluids and Plasmas Collection

READ NOW



Thermal stability of α -Ga₂O₃ films grown on c-plane sapphire substrates via mist-CVD

Cite as: AIP Advances 10, 115013 (2020); doi: 10.1063/5.0020464

Submitted: 10 October 2020 • Accepted: 15 October 2020 •

Published Online: 10 November 2020



View Online



Export Citation



CrossMark

Riena Jinno,^{1,a)}  Kentaro Kaneko,^{1,2,3}  and Shizuo Fujita^{1,2,a)} 

AFFILIATIONS

¹Department of Electronics Science and Engineering, Kyoto University, Kyoto 615-8510, Japan

²Photonics and Electronics Science and Engineering Center, Kyoto University, Kyoto 615-8520, Japan

³Engineering Education Research Center, Kyoto University, Kyoto 615-8530, Japan

^{a)}Authors to whom correspondence should be addressed: jinno.riena.t69@kyoto-u.jp and fujitasz@kuee.kyoto-u.ac.jp

ABSTRACT

The thermal stability of α -Ga₂O₃ films grown on c-plane sapphire substrates was investigated. A strong correlation was found between thermal stability and film thickness: the more the α -Ga₂O₃ films maintained the α -phase upon heating at higher annealing temperature, the thinner they were. Transmission electron microscopy observations revealed that the phase transition of the α -Ga₂O₃ film to the thermodynamically most stable β -phase had the orientation relationship of β -Ga₂O₃ [201] || sapphire [0001]. High-temperature x-ray diffraction measurement for the α -Ga₂O₃ film showed the relationship of β -Ga₂O₃ [401]/[301] || sapphire [0001] as well. The dependence of the stability boundary on the film thickness originates from a thermal stress caused by a larger thermal expansion coefficient of α -Ga₂O₃ than that of sapphire. Relaxation of residual stress by introducing a selective area growth technique enhanced the thermal stability of α -Ga₂O₃ so that α -Ga₂O₃ maintained the corundum structure upon heating at 800 °C, although a small diffraction peak from β -Ga₂O₃ was detected by x-ray diffraction measurement. The enhanced thermal stability of α -Ga₂O₃ widens device process windows as well as growth windows.

© 2020 Author(s). All article content, except where otherwise noted, is licensed under a Creative Commons Attribution (CC BY) license (<http://creativecommons.org/licenses/by/4.0/>). <https://doi.org/10.1063/5.0020464>

Ga₂O₃ is an ultra-wide bandgap (UWBG) semiconductor material suitable for high-power and high-voltage device applications due to its estimated large breakdown field.^{1–3} Among the five different polymorphs of Ga₂O₃ (α , β , γ , δ , and ϵ), the β -gallia structure is the thermodynamically most stable phase.^{4,5} Most studies of Ga₂O₃ are related to the β -phase because high quality β -Ga₂O₃ free-standing substrates can be made by several melting methods^{6–12} leading to demonstrations of both lateral and vertical devices using the homoepitaxial growth of β -Ga₂O₃.^{13–18} On the other hand, in recent years, metastable α -Ga₂O₃ with the trigonal corundum structure has attracted much interest as well. Single-crystalline α -Ga₂O₃ films are successfully grown on inexpensive sapphire substrates using mist chemical vapor deposition (CVD)^{19–22} and halide vapor phase epitaxy (HVPE),^{23,24} overcoming the difficulty associated with semi-stable behavior in crystal growth. In addition, α -Ga₂O₃ forms alloys with Al₂O₃, spanning experimental bandgaps of ~5.3 eV–8.6 eV,^{25,26} while the highest Al content of β -(Al_xGa_{1-x})₂O₃ epitaxial films is experimentally reported to be $x \sim 0.77$ ($E_g \sim 6.4$ eV).^{27,28} However, metastable α -Ga₂O₃

has a propensity to revert to the thermodynamically most stable β -phase: α -Ga₂O₃ has been reported to convert to the β -phase upon heating at atmospheric pressure at 600 °C–650 °C.^{4,5,29,30} This is a severe limitation for fabrication of α -Ga₂O₃-based devices because it means that the temperature of the film has to be set lower than 600 °C throughout device processing. In particular, doping α -Ga₂O₃ by ion-implantation has not been achieved yet due to the low phase transition temperature. Si-ion implantation in β -Ga₂O₃ has been activated at 900 °C–1000 °C.³¹ A similar activation annealing temperature is predicted to be required for ion implantation in α -Ga₂O₃, but it is higher than the phase transition temperature of α -Ga₂O₃. Against the phase transition temperature of around 600 °C, the growth of α -Ga₂O₃ films has been achieved at a thermocouple growth temperature of 800 °C,³² suggesting that α -Ga₂O₃ can maintain the corundum structure at a temperature higher than 650 °C by some techniques. C-plane sapphire substrates are generally used for the growth of α -Ga₂O₃ via mist-CVD and HVPE;^{19,21–23,33,34} hence, in this study, we report the enhancement of thermal stability of α -Ga₂O₃ films grown on c-plane sapphire at

up to 800 °C by decreasing the film thickness and utilizing the selective area growth technique. The mechanism of phase transition of the α -Ga₂O₃ films to the thermodynamically most stable β -phase is discussed.

α -Ga₂O₃ films were grown on c-plane sapphire substrates using mist-CVD.^{2,20–22} Gallium(III) trichloride (GaCl₃) or gallium(III) acetylacetonate [Ga(acac)₃] was dissolved in a mixed solution of H₂O and HCl. For growth via mist-CVD, Ga(acac)₃ introduces a high carbon concentration of 10¹⁹ cm⁻³ in the α -Ga₂O₃ film,²¹ while GaCl₃ offers a low impurity concentration.³³ N₂ was used as both the carrier and the dilution gas. The growth temperature (T_g) was set between 500 °C and 700 °C. Note that T_g is the thermocouple temperature monitoring the outer wall of the quartz tube in the hot-wall type mist-CVD system. The α -Ga₂O₃ films were post-annealed in an atmospheric furnace at annealing temperatures (T_A) between 600 °C and 750 °C after growth, using a Denken Muffle furnace KDF-S70G. The samples were heated from room temperature to T_A in 1 h (a heating rate of ~9.5 °C/min–12 °C/min), kept at T_A for 30 min, and then naturally cooled to room temperature. After annealing, the phase stability of the α -Ga₂O₃ films against the thermal treatment was investigated by symmetric x-ray diffraction (XRD) $2\theta/\omega$ measurements using a Rigaku ATX system at room temperature. High-temperature XRD (HT-XRD) with a Rigaku SmartLab system was used to investigate the thermal stability of the α -Ga₂O₃ films as well as to assess lattice lengths of the α -Ga₂O₃ films and sapphire substrates. The HT-XRD measurement gives phase information at a given temperature *in situ*. The HT-XRD measurement was carried out under an air atmosphere; after the growth, the samples were placed on a black synthetic quartz glass of the HT-XRD system, and the thermocouple temperature (T_H) was monitored. The heating rates were 50 °C/min and 10 °C/min for $T_H \leq 600$ °C and $T_H > 600$ °C, respectively. The samples were kept at T_H for ~10 min before each scan so that the diffractometer axis could be aligned. In this study, monochromatic Cu K α_1 radiation ($\lambda = 1.54056$ Å) was used for all XRD measurements.

Figure 1 shows an example of the variations in symmetric XRD $2\theta/\omega$ scan profiles of the α -Ga₂O₃ films, with thicknesses of 110 nm–140 nm, before and after annealing at T_A . It can be seen that the film maintained the corundum structure at $T_A \leq 660$ °C, while at $T_A = 670$ °C, a weak diffraction peak originated from β -Ga₂O₃ 402. The α -Ga₂O₃ film gradually changed to the β -phase at $T_A \geq 670$ °C, at which the diffraction peaks from both the α - and β -phases were detected and completely converted to β -Ga₂O₃ at $T_A = 700$ °C. The gradual transition to the β -phase was also reported in the previous study by Lee *et al.*²⁹

Thermal annealing processes and XRD measurements were conducted for a range of different growth conditions. The thermal stability of the samples is summarized in Fig. 2. In this study, we investigated α -Ga₂O₃ films with thicknesses greater than 20 nm. Since the critical thickness of α -Ga₂O₃ films grown on c-plane sapphire substrates is expected to be a few nm due to the large lattice mismatch between sapphire and α -Ga₂O₃ (4.6% along the a-axis),³⁵ the α -Ga₂O₃ films used here were almost fully relaxed even when the thickness was as thin as about 20 nm, as revealed by reciprocal space maps for the α -Ga₂O₃ films [Fig. S1]. Open and solid symbols show samples that maintained the α -phase or completely converted to β -Ga₂O₃, respectively, revealed from XRD $2\theta/\omega$ scan profiles.

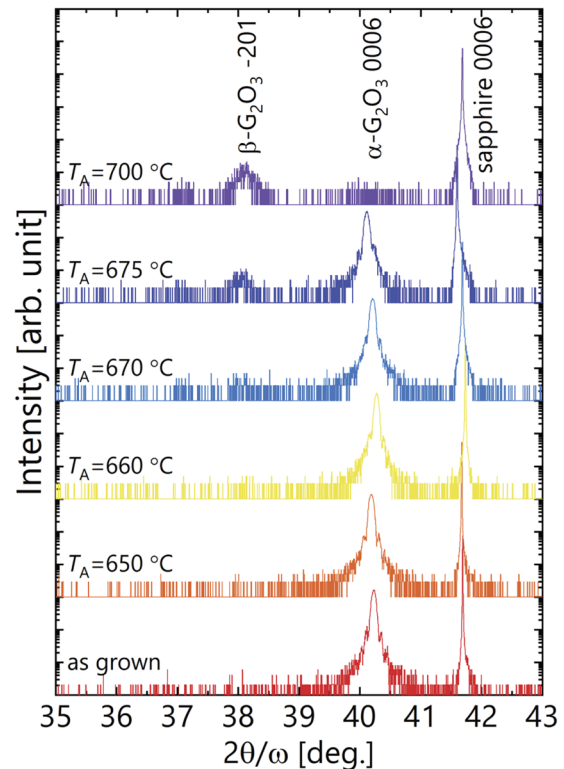


FIG. 1. Symmetric XRD $2\theta/\omega$ scan profiles of the Ga₂O₃ films with a film thickness of 110 nm–140 nm on c-plane sapphire substrates before and after annealing at 650 °C, 660 °C, 670 °C, 675 °C, and 700 °C.

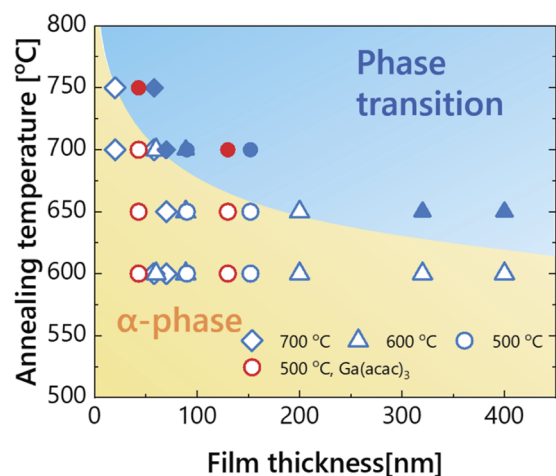


FIG. 2. Open symbols indicate samples that maintained the α -phase, and solid symbols indicate samples that completely converted to the β -phase at an annealing temperature as a function of film thickness. Samples drawn in red and blue colors were grown using Ga(acac)₃ and GaCl₃, respectively, as a Ga precursor. The circular, triangular, and rhomboid symbols show the growth temperature of 500 °C, 600 °C, and 700 °C, respectively.

The phase transition temperature to the β -phase correlated strongly with the film thickness but barely correlated with the growth temperature T_g and the Ga precursor. When thicker than $1\ \mu\text{m}$, the α - Ga_2O_3 films converted to the β -phase at $T_A = 600^\circ\text{C}$, as reported by Lee *et al.*²⁹ With thinner films, the α - Ga_2O_3 films maintained the corundum structure at temperatures higher than 600°C . An α - Ga_2O_3 film around $20\ \text{nm}$ thick maintained the corundum structure at $T_A = 750^\circ\text{C}$, which was 150°C higher than that of a film several hundred nm thick. The dependence of the phase transition temperature on the film thickness allowed the growth of α - Ga_2O_3 films at $T_g > 600^\circ\text{C}$ provided they were thin.³²

Transmission electron microscope (TEM) observation was conducted to explore how the α - Ga_2O_3 film grown on sapphire converted to the β -phase under thermal treatment. We observed a sample around $135\ \text{nm}$ thickness that had been annealed at $T_A = 670^\circ\text{C}$ for $30\ \text{min}$, after which it had partially converted to β - Ga_2O_3 , as revealed by the XRD $2\theta/\omega$ scan profile [Fig. 1]. For $T_A = 660^\circ\text{C}$, no other phases were observed from the TEM observation, corresponding to the result of the XRD. The details for $T_A = 660^\circ\text{C}$ are described in the [supplementary material](#) [Fig. S1]. Figure 3(a) is an overview of a cross-sectional dark-field TEM image of the α - Ga_2O_3 film annealed at $T_A = 670^\circ\text{C}$ viewed along the $11\bar{2}0$ axis. Figures 3(b) and 3(c) are the high magnification dark- and bright-field TEM images, respectively, for yellow box (1) in Fig. 3(a). These images

reveal that a semielliptic different phase/domain, which is schematically illustrated in Fig. 3(d), was introduced in the vicinity of the surface. In the bright field image [Fig. 3(b)], the semielliptic area showed several different contrasts. Diffraction patterns for the sapphire substrate, for the film in the vicinity of the interface, and in the semielliptic region were taken to investigate the crystal structures of each area. The diffraction pattern for the film at the interface has the same pattern as that for the substrate [Figs. 3(e) and 3(f)], showing the single-crystalline α -phase, while the patterns for the semielliptic regions are identified as that of β - Ga_2O_3 [Figs. 3(g) and 3(h)]. The orientation relationship is β - Ga_2O_3 $[\bar{2}01] \parallel \alpha$ - Ga_2O_3 $[0001]$. β - Ga_2O_3 grown on c-plane sapphire also has been reported to have the same epitaxial relationship: β - Ga_2O_3 $[\bar{2}01] \parallel \text{sapphire}$ $[0001]$.^{35,36} Figure 3(h) clearly shows the $[102]$ projected diffraction pattern for the β -phase, while Fig. 3(g) depicts several patterns viewed along various directions with an orientation relationship of β - Ga_2O_3 $[\bar{2}01] \parallel \text{sapphire}$ $[0001]$. This indicates that there are overlapping rotational domains in (g), as shown in Fig. 3(c), which caused the different contrast in the TEM images for (g) and (h) in Fig. 3(c). In the α - Ga_2O_3 layer, high-density dislocations extended from the grown interface to the surface of the film, appearing as white lines in the dark-field image [Fig. 3(b)]. Figure 3(i) shows a magnification of the red box in Fig. 3(c). The α - Ga_2O_3 lattice structure looks strained around the dislocations, but an introduction of different phases/domains is not detected. The phase transition arising from the dislocations

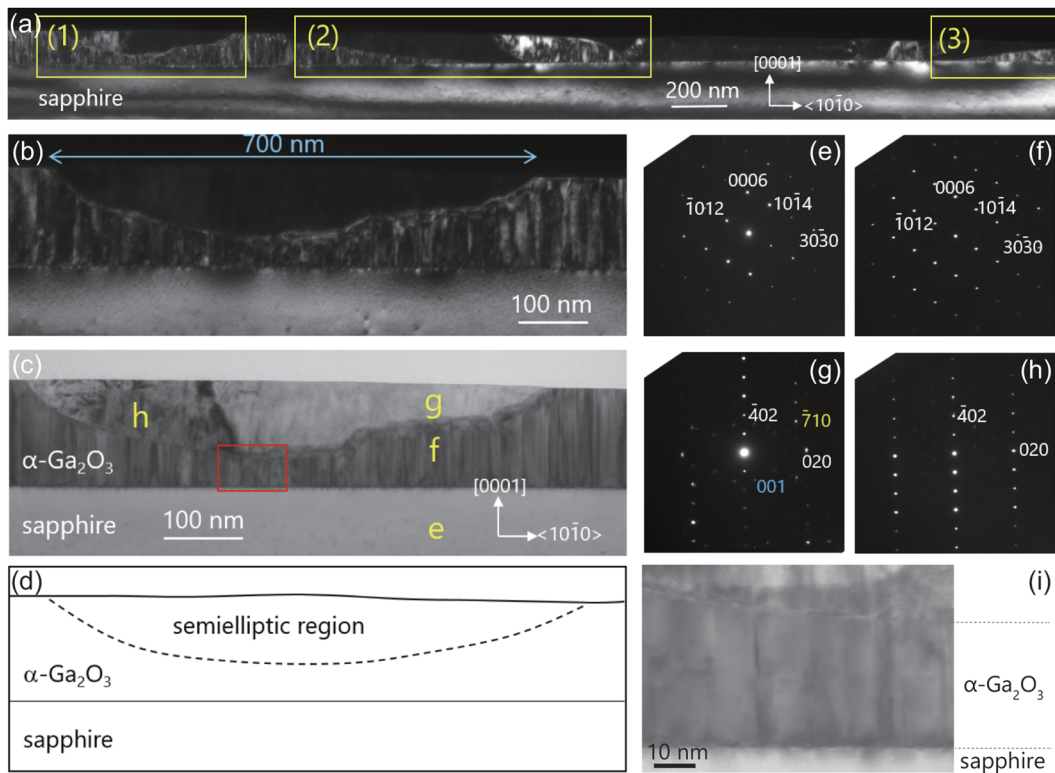


FIG. 3. (a) Cross-sectional dark field TEM image of the $135\ \text{nm}$ α - Ga_2O_3 film on the sapphire substrate after annealing at 670°C viewed along the $11\bar{2}0$ axis. (b) Dark field, (c) bright-field, and (d) schematic images for yellow box (1) shown in (a). (e)–(h) are diffraction spots for the area shown in (c). (i) Magnification of the red box shown in (c).

was not clearly observed from the present *ex situ* TEM observation. However, the high dislocation density in α -Ga₂O₃ could be crucial in defining the phase stability boundary, and further study using *in situ* TEM will be required to investigate the starting point of the phase transition. The TEM observations conducted for yellow boxes (2) and (3) also show the phase transition to β -Ga₂O₃ in the black regions in the α -Ga₂O₃ film shown in Fig. 3(a). The details are shown in the supplementary material [Fig. S2]. Although overlapping of α - and β -Ga₂O₃ makes the phase transition boundary look disordered, by the present thermal treatment, the TEM observations do not show disordered regions, suggesting the direct transition of the α -phase to the β -phase without an intermediate step. However, different heating/cooling rates in the annealing process might result in an intermediate step or conversion to other polymorphs such as the γ -phase, as reported in the study of the phase transformation of ϵ -Ga₂O₃ by Cora *et al.*³⁷

The phase stability of α -Ga₂O₃ layers grown on sapphire substrates was also investigated using HT-XRD measurements. We prepared two different α -Ga₂O₃ films grown under the same growth condition: one uniformly grown on a substrate with a thickness of about 120 nm and the other selective-area grown (SAG) α -Ga₂O₃ with a thickness of about 500 nm. The SAG film was grown using a dot-patterned SiO₂ mask where the diameter of the dots was 3 μ m, on a c-plane sapphire substrate [Fig. 4(a)]. The film thickness of the SAG α -Ga₂O₃ was about 500 nm, as revealed by a cross-sectional scanning electron microscope (SEM) [Fig. 4(b)], several times as thick as that of the uniformly grown film (about 120 nm) due to the incorporation of source materials supplied on the mask into the α -Ga₂O₃ facet on the window area. SAG α -Ga₂O₃ fabrication via mist-CVD was reported in the previous study.³⁸ Enhancement of the thermal phase stability of α -Ga₂O₃ is expected by adopting SAG since it leads to reducing the dislocation density in the α -Ga₂O₃ layer, especially in the masked region [Fig. S4], as well as the thermal stress induced by the difference between the thermal expansion coefficient of sapphire and that of α -Ga₂O₃.

Phase transformation of the α -Ga₂O₃ film starts at $T_H = 660$ °C, showing diffraction peaks from β -Ga₂O₃ 402 and 401/310 [Fig. 4(c)]. The transition to the β -phase with orientation 401 or 310 with respect to the sapphire substrate is not detected by the XRD study conducted for the samples after annealing at T_A [Fig. 1] probably because of the different heating rates and/or the phase information at room temperature of the samples after annealing. The film is completely converted to β -Ga₂O₃ at $T_H = 720$ °C–740 °C. The difference between *ex situ* (T_A) and *in situ* (T_H) phase transition temperatures arises from using a different annealing system as well as the different heating/cooling rates. On the other hand, the SAG α -Ga₂O₃ layer shows a small diffraction peak from β -Ga₂O₃ at $T_H = 680$ °C–700 °C, but the diffraction peak from α -Ga₂O₃ 0006 still clearly remains upon heating at $T_H = 800$ °C [Fig. 4(d)]. The weak intensity from the β -Ga₂O₃ reflexes suggests that the dislocation concentrated α -Ga₂O₃ layer above the mask region did not completely convert to the β -phase. The SAG α -Ga₂O₃ was also exposed to thermal annealing at $T_A = 800$ °C for 10 h, and the XRD profile was measured by the Rigaku ATX system. The uniformly grown α -Ga₂O₃ film with a thickness of a few hundred nm completely converted to the β -phase after annealing at $T_A = 650$ °C for 30 min [Fig. 2]. On the other hand, the intensity of the diffraction peak from the β -phase does not increase, and the SAG α -Ga₂O₃

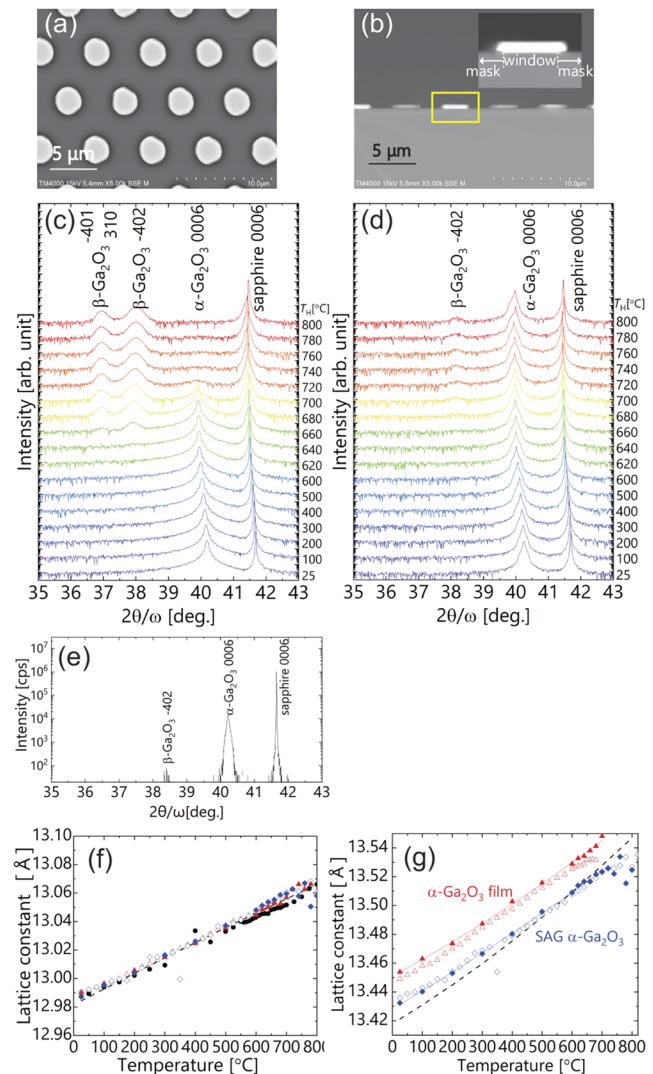


FIG. 4. (a) Bird's-eye and (b) cross-sectional SEM images of the SAG α -Ga₂O₃ on c-plane sapphire with a 3 μ m-diameter dot-patterned mask, symmetric high temperature XRD $2\theta/\omega$ scan profiles for (c) the α -Ga₂O₃ film and (d) the SAG α -Ga₂O₃ in the temperature range of 25 °C–800 °C, and (e) the symmetric XRD $2\theta/\omega$ scan profile of the SAG Ga₂O₃ after annealing at $T_A = 800$ °C for 10 h. The c lattice parameter of (f) sapphire and (g) α -Ga₂O₃ obtained using high temperature XRD. The red triangles, blue diamonds, and black circles show the parameters of the α -Ga₂O₃ film, the SAG α -Ga₂O₃ on c-plane sapphire, and a c-plane sapphire as received, respectively. The black dashed lines show the reported values in the previous studies.

keeps the corundum structure after annealing at $T_A = 800$ °C for 10 h [Fig. 4(e)]. These results indicate that the thermal stability of α -Ga₂O₃ is dramatically enhanced by using the SAG technique, as expected.

From the diffraction peak positions of the HT-XRD scan profiles, lattice parameters (c) and thermal expansion coefficients (α) of the α -Ga₂O₃ layers and the sapphire substrates were calculated as second-order polynomials by regression analysis of the data

TABLE I. Temperature variation of lattice parameters (c) and thermal expansion coefficients (α) of sapphire and α -Ga₂O₃.

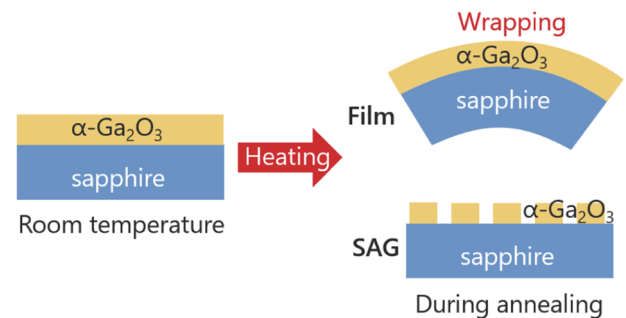
Material		c [Å]	α [°C]
Sapphire	SAG	$12.985 + 9.721 \times 10^{-5}T + 1.498 \times 10^{-8}T^2$	$7.487 \times 10^{-6} + 2.252 \times 10^{-9}T - 2.814 \times 10^{-14}T^2$
	FILM	$12.988 + 7.973 \times 10^{-5}T + 2.711 \times 10^{-8}T^2$	$6.141 \times 10^{-6} + 4.136 \times 10^{-9}T - 4.747 \times 10^{-14}T^2$
	Reference 39	$12.9815 + 11.2939 \times 10^{-5}T - 9321 \times 10^{-9}T^2$	8.11×10^{-6} (20 °C–800 °C)
α -Ga ₂ O ₃	SAG	$13.4282 + 1.236 \times 10^{-4}T + 1.895 \times 10^{-8}T^2$	$8.338 \times 10^{-6} + 4.681 \times 10^{-9}T - 7.0116 \times 10^{-14}T^2$
	FILM	$13.4511 + 1.122 \times 10^{-4}T + 3.193 \times 10^{-8}T^2$	$9.206 \times 10^{-6} + 2.739 \times 10^{-9}T - 4.203 \times 10^{-14}T^2$
	Reference 40	$13.4178 + 1.254 \times 10^{-4}T + 4.478 \times 10^{-8}T^2$	$9.347 \times 10^{-6} + 6.591 \times 10^{-9}T + 4.478 \times 10^{-14}T^2$

(Table I). As a reference, the XRD measurement was also conducted for a bare c -plane sapphire substrate. In order to show the reproducibility of the measurement as well as investigate the lattice parameters in detail, we also conducted HT-XRD measurements for the α -Ga₂O₃ layers with smaller temperature intervals. For $T_H < 600$ °C, an interval (heating rate) of 25 °C was used, and for $T_H \geq 600$ °C, 10 °C, and 20 °C were adopted for the α -Ga₂O₃ film and the SAG α -Ga₂O₃, respectively. The measured lattice parameter (c) of the c -plane sapphire substrates agreed well with that reported by Yim, not changed by the growth of α -Ga₂O₃ [Fig. 4(f)].³⁹ The lattice length of the SAG α -Ga₂O₃ layer was close to the reported value,⁴⁰ while the α -Ga₂O₃ film showed a ~ 0.02 Å longer lattice parameter than that of the reported one in the entire range of T_H [Fig. 4(g)]. The α -Ga₂O₃ film was not completely relaxed and was subject to slight in-plane compressive strain at room temperature after growth due to the thin film thickness of around 120 nm, which was observed for the sample grown at $T_g > 600$ °C. The dependence of the α -Ga₂O₃ growth on growth temperature will be reported in detail elsewhere. The calculated thermal expansion coefficients of all the samples were slightly smaller than the value in the previous study, but they were larger than that of sapphire (Table I).

The phase stability of α -Ga₂O₃ on c -plane sapphire was enhanced by decreasing the film thickness and utilizing the SAG technique. The α -Ga₂O₃ films used here were almost fully relaxed even when the thickness was as thin as around 20 nm [Fig. S1], indicating similarly high density of dislocations in thicker α -Ga₂O₃ films. The dislocation density in a α -Ga₂O₃ layer on c -plane sapphire has been reported to be in the order of 10^{10} cm⁻².^{20,34} In addition, the dense dislocation α -Ga₂O₃ area grown in the window region did not completely transform to β -Ga₂O₃ at $T_A/T_H = 800$ °C, even though the thickness was as large as 500 nm. From these results, it can be concluded that the dislocation density in α -Ga₂O₃ was not defining the stability boundary of α -Ga₂O₃ on sapphire at the present stage and another factor such as the thermal stress in α -Ga₂O₃ is likely to be contributing to the phase transformation to β -Ga₂O₃. However, such defects could be the starting point of the phase transformation to the β -phase and be crucial for phase stability. Experimentally, α -Ga₂O₃ has a larger thermal expansion coefficient than that of sapphire, and the difference of the coefficients becomes larger at higher temperature,^{39,40} leading to a strain in α -Ga₂O₃ as well as sapphire, as shown schematically in Fig. 5. The experimental thermal expansion coefficient in this study also showed the same tendency. By decreasing the film thickness or using the selective area growth, the stress can be released, resulting in the

enhancement of phase stability. It is also possible that the phase transition to the β -phase arises from an inhomogeneous strain in α -Ga₂O₃. At the present stage, the small amount of β -Ga₂O₃ is included in the SAG α -Ga₂O₃ after annealing, but the inclusion is probably due to the strain on the window region where α -Ga₂O₃ is subject to the strain from the sapphire substrate. This suggests that a free-standing high-quality α -Ga₂O₃ bulk maintains the corundum structure at temperatures higher than 800 °C without undesirable phase conversion.

In conclusion, the thermal stability of α -Ga₂O₃ films and an SAG α -Ga₂O₃ on c -plane sapphire substrates was investigated in this study. The XRD results conducted at room temperature for the samples after annealing at T_A revealed that the phase transition temperature of the α -Ga₂O₃ films increased as the film thickness decreased, regardless of the growth conditions. The TEM observations for the α -Ga₂O₃ film revealed phase transition to the β -phase with the orientation relationship of β -Ga₂O₃ [201] || α -Ga₂O₃/sapphire [0001]. The HT-XRD measurement gave phase information at a given temperature *in situ* and showed that the α -Ga₂O₃ film converted to the β -phase in the same annealing temperature range as that observed in the XRD measurement for the samples after annealing at T_A , but the orientation [401]/[301] of β -Ga₂O₃ parallel to [0001] of α -Ga₂O₃/sapphire was detected as well. In addition, the SAG α -Ga₂O₃ enhanced the thermal stability of α -Ga₂O₃, maintaining the α -phase after annealing at 800 °C for 10 h, although a small diffraction peak from the β -phase was observed in the XRD profile. The strain arising from the difference between the thermal expansion coefficient

**FIG. 5.** Schematics of the relationship between an α -Ga₂O₃ film/SAG α -Ga₂O₃ and a sapphire substrate at room temperature and at annealing temperature.

of sapphire and that of α -Ga₂O₃ is likely to be crucial for the phase stability boundary. From these results, α -Ga₂O₃ is expected to maintain a corundum structure at temperatures higher than 800 °C by removing the stress in α -Ga₂O₃ by, for example, the fabrication of α -Ga₂O₃ bulk grown by using the epitaxial lateral overgrowth technique.

See the [supplementary material](#) for the reciprocal space maps and TEM observations.

Part of this work was supported by the Advanced Research Program for Energy and Environmental Technologies of the New Energy and Industrial Technology Development Organization (NEDO). The authors would like to sincerely thank Professor Katsuhisa Tanaka of Kyoto University for providing the high-temperature XRD system and useful discussions with him. They also acknowledge helpful discussions with Professor Toshiyuki Kawaharamura.

DATA AVAILABILITY

The data that support the findings of this study are available from the corresponding author upon reasonable request.

REFERENCES

- ¹M. Higashiwaki, H. Murakami, Y. Kumagai, and A. Kuramata, *Jpn. J. Appl. Phys.* **55**, 1202A1 (2016).
- ²S. Fujita, M. Oda, K. Kaneko, and T. Hitora, *Jpn. J. Appl. Phys.* **55**, 1202A3 (2016).
- ³S. J. Pearton, J. Yang, P. H. Cary, F. Ren, J. Kim, M. J. Tadjer, and M. A. Mastro, *Appl. Phys. Rev.* **5**, 011301 (2018).
- ⁴R. Roy, V. G. Hill, and E. F. Osborn, *J. Am. Chem. Soc.* **74**, 719 (1952).
- ⁵H. Y. Playford, A. C. Hannon, E. R. Barney, and R. I. Walton, *Chem. - Eur. J.* **19**, 2803 (2013).
- ⁶N. Ueda, H. Hosono, R. Waseda, and H. Kawazoe, *Appl. Phys. Lett.* **70**, 3561 (1997).
- ⁷E. G. Villora, K. Shimamura, Y. Yoshikawa, K. Aoki, and N. Ichinose, *J. Cryst. Growth* **270**, 420 (2004).
- ⁸N. Suzuki, S. Ohira, M. Tanaka, T. Sugawara, K. Nakajima, and T. Shishido, *Phys. Status Solidi* **4**, 2310 (2007).
- ⁹E. G. Villora, K. Shimamura, Y. Yoshikawa, T. Ujiie, and K. Aoki, *Appl. Phys. Lett.* **92**, 202120 (2008).
- ¹⁰H. Aida, K. Nishiguchi, H. Takeda, N. Aota, K. Sunakawa, and Y. Yaguchi, *Jpn. J. Appl. Phys.* **47**, 8506 (2008).
- ¹¹Y. Tomm, P. Reiche, D. Klimm, and T. Fukuda, *J. Cryst. Growth* **220**, 510 (2000).
- ¹²Z. Galazka, R. Uecker, K. Irmischer, M. Albrecht, D. Klimm, M. Pietsch, M. Brützmam, R. Bertram, S. Ganschow, and R. Fornari, *Cryst. Res. Technol.* **45**, 1229 (2010).
- ¹³M. Higashiwaki, K. Sasaki, A. Kuramata, T. Masui, and S. Yamakoshi, *Appl. Phys. Lett.* **100**, 013504 (2012).
- ¹⁴M. Higashiwaki, K. Sasaki, T. Kamimura, M. Hoi Wong, D. Krishnamurthy, A. Kuramata, T. Masui, and S. Yamakoshi, *Appl. Phys. Lett.* **103**, 123511 (2013).
- ¹⁵K. Konishi, K. Goto, H. Murakami, Y. Kumagai, A. Kuramata, S. Yamakoshi, and M. Higashiwaki, *Appl. Phys. Lett.* **110**, 103506 (2017).
- ¹⁶M. H. Wong, Y. Nakata, A. Kuramata, S. Yamakoshi, and M. Higashiwaki, *Appl. Phys. Express* **10**, 041101 (2017).
- ¹⁷Z. Hu, K. Nomoto, W. Li, Z. Zhang, N. Tanen, Q. T. Thieu, K. Sasaki, A. Kuramata, T. Nakamura, D. Jena, and H. G. Xing, *Appl. Phys. Lett.* **113**, 122103 (2018).
- ¹⁸W. Li, Z. Hu, K. Nomoto, R. Jinno, Z. Zhang, T. Q. Tu, K. Sasaki, A. Kuramata, D. Jena, and H. G. Xing, in *2018 IEEE International Electron Devices Meet (IEEE, 2018)*, pp. 8.5.1–8.5.4.
- ¹⁹D. Shinohara and S. Fujita, *Jpn. J. Appl. Phys.* **47**, 7311 (2008).
- ²⁰K. Kaneko, H. Kawanowa, H. Ito, and S. Fujita, *Jpn. J. Appl. Phys.* **51**, 020201 (2012).
- ²¹K. Akaiwa and S. Fujita, *Jpn. J. Appl. Phys.* **51**, 070203 (2012).
- ²²T. Kawaharamura, G. T. Dang, and M. Furuta, *Jpn. J. Appl. Phys.* **51**, 040207 (2012).
- ²³Y. Oshima, E. G. Villora, and K. Shimamura, *Appl. Phys. Express* **8**, 055501 (2015).
- ²⁴E. Ahmadi and Y. Oshima, *J. Appl. Phys.* **126**, 160901 (2019).
- ²⁵H. Ito, K. Kaneko, and S. Fujita, *Jpn. J. Appl. Phys.* **51**, 100207 (2012).
- ²⁶G. T. Dang, T. Yasuoka, Y. Tagashira, T. Tadokoro, W. Theiss, and T. Kawaharamura, *Appl. Phys. Lett.* **113**, 062102 (2018).
- ²⁷T. Oshima, T. Okuno, N. Arai, Y. Kobayashi, and S. Fujita, *Jpn. J. Appl. Phys.* **48**, 070202 (2009).
- ²⁸C.-L. Liao, K.-H. Li, C. G. Torres-Castanedo, G. Zhang, and X. Li, “ β -phase (AlxGa1-x)2O3 thin film with Al composition more than 70%,” [arXiv:2005.05799v2](#).
- ²⁹S.-D. Lee, K. Akaiwa, and S. Fujita, *Phys. Status Solidi* **10**, 1592 (2013).
- ³⁰S.-D. Lee, Y. Ito, K. Kaneko, and S. Fujita, *Jpn. J. Appl. Phys.* **54**, 030301 (2015).
- ³¹K. Sasaki, M. Higashiwaki, A. Kuramata, T. Masui, and S. Yamakoshi, *Appl. Phys. Express* **6**, 086502 (2013).
- ³²R. Jinno, T. Uchida, K. Kaneko, and S. Fujita, *Phys. Status Solidi* **255**, 1700326 (2018).
- ³³M. Oda, R. Tokuda, H. Kambara, T. Tanikawa, T. Sasaki, and T. Hitora, *Appl. Phys. Express* **9**, 021101 (2016).
- ³⁴Y. Oshima, K. Kawara, T. Shinohe, T. Hitora, M. Kasu, and S. Fujita, *APL Mater.* **7**, 022503 (2019).
- ³⁵R. Schewski, G. Wagner, M. Baldini, D. Gogova, Z. Galazka, T. Schulz, T. Remmele, T. Markurt, H. von Wenckstern, M. Grundmann, O. Bierwagen, P. Vogt, and M. Albrecht, *Appl. Phys. Express* **8**, 011101 (2015).
- ³⁶T. Oshima, T. Okuno, and S. Fujita, *Jpn. J. Appl. Phys.* **46**, 7217 (2007).
- ³⁷I. Cora, Z. Fogarassy, R. Fornari, M. Bosi, A. Rečnik, and B. Pécz, *Acta Mater.* **183**, 216 (2020).
- ³⁸R. Jinno, N. Yoshimura, K. Kaneko, and S. Fujita, *Jpn. J. Appl. Phys.* **58**, 120912 (2019).
- ³⁹W. M. Yim and R. J. Paff, *J. Appl. Phys.* **45**, 1456 (1974).
- ⁴⁰L. J. Eckert and R. C. Bradt, *J. Am. Ceram. Soc.* **56**, 229 (1973).